A Fast PV MPPT Scheme using Boundary Control with Second-order Switching Surface

Y. Zhou, *Student Member, IEEE*, Carl N. M. Ho, *Senior Member, IEEE*, and Ken K. M. Siu, *Student Member, IEEE*

Abstract — The continuously increasing demand of renewable energy has advanced the development of Photovoltaic (PV) systems and Maximum Power Point Tracking (MPPT) algorithms. Classic hill-climbing plus PI technique is being challenged under rapidly changing environmental conditions. This paper proposes a MPPT algorithm with fast transient responses while maximizing the efficiency of PV application. This novel approach employs a dp/dv tracking method in conjunction with a second-order switching surface controller in a boost-type converter. Successful tracking of MPP is achieved in switching-cycle level with a precise voltage ripple control. A 280W converter embedded with the proposed controller is built and tested with multiple PV panels. Experiment results show the proposed scheme can reach new MPP in 300us and show a good agreement with the derived theory.

Keywords— MPPT, PV, dp/dv tracker, boundary control

I.   INTRODUCTION

Solar energy is an environmental friendly renewable energy resource and considers as a suitable solution to mitigate in the energy crisis. Photovoltaic is a technique which can directly convert solar energy into electricity using semiconducting materials without having impacts on the environment during the conversion [2]. PV applications are widely used in the power supply state of the aerospace application [3], and are also commonly seen as a standalone systems in remote communities or residence houses [4]. As an important component in a microgrid, PV systems can supply local loads or feed the energy back to the grid via power electronic interfaces [5]-[6]. Due to the nonlinear I-V characteristic of PV panel, the maximum power point (MPP) is required to be tracked by a MPPT controller to ensure PV system is operating at the point [7]. Thus, under variation of solar irradiation, cloud coverage and temperature conditions, the maximum output power of PV is able to be guaranteed. With a MPPT controller, maximum power can be extracted from PV panels, hence the conversion efficiency of PV is boosted and the cost of produced PV energy is reduced [8]. Furthermore, under rapidly changing environmental conditions, a MPPT with a fast dynamic response performance is essential. EN50530 [9] is generally applied to evaluate the dynamic performance of MPPT controller in a specified varying irradiance sequence.

Numerous MPPT algorithms are presented in literature, where Perturb and Observe (P&O) is one of the most popular one used in industry due to its simplicity and economic merits

Y. Zhou is with Hatch Ltd., 330 St Mary Ave #500, R3C 3Z5, Winnipeg, MB, Canada.

C.N.M. Ho (Corresponding author) and K.K.M Siu are with the Department of Electrical & Computer Engineering, University of Manitoba, R3T5V6, Winnipeg, MB, Canada (E-mail: carl.ho@umanitoba.ca).

of implementation [10]-[11]. Notice that, the step size of the perturbation is determined from the trade-off between the MPPT accuracy and speed of MPP tracking [12]-[13]. Another popular MPPT control technique is incremental conductance (INC), which is more accurate to than the P&O and track MPP with oscillation-free at MPP [14]-[15]. The constant voltage method is another method. The bright side of it is less number of sensing signal is required, only PV voltage is sensed. However, this method is limited by environmental conditions [16]. Dynamic performance of fuzzy logic control in [17] is improved but still limited to milliseconds level.

Proportional Integral (PI) controller is typically applied conjointly with MPPT algorithms to modulate the duty ratio in a PV converter. However, the transient response of such controller is not optimized [18]-[19]. Particularly for a reconfigurable PV array [20] and fast moving objects such as PV mounted vehicle or aircraft, where PI controller fails to establish new operating point under rapid changing irradiance. This results that the operation point does not coincide with the actual MPP due to the delay of controller response. Thus, the MPPT output power efficiency is reduced and poor tracking accuracy is resultant. In addition, the slow MPPT takes a longer time to reach new MPP. For a large-scale PV farm, the power loss during this transient can be significant.

This paper proposes a fast MPPT control scheme based on a boost converter with dual loop control to maximize power generation from PV panels. This control scheme, *dp/dv* of PV power-voltage curve is used to track MPP and boundary controller is utilized to fastly modulate the PV output voltage. In contrast to PI-based MPPT, proposed controller guides the operation point towards new MPP in a few hundred microseconds instead of millisecond range, typically for conventional MPPT algorithms. Also it keeps a stable operation during steady state [19]. The technical contributions of the paper are, 1) to achieve fast MPPT tracking performance, a concept of cascading *dp/dv* tracker and boundary controller is proposed and derived, 2) it is first time to applying boundary control with second-order switching surface into MPPT for PV applications with the supported by simulation and experiment results, and 3) the overall system steady state characteristics have been determined and have been proofed. The principle of operation, controller design, simulation and experimental results will be discussed in the following sections.

II.   PRINCIPLES OF OPERATION

Converter topology is essential to realize MPPT, among various DC/DC converters, boost-type converter is a widely used topology [21]. It is because 1) of the simplicity and easiness of implementation, 2) the typical output voltage of the converter, for example dc link voltage, is generally higher than the PV

string voltage and 3) input current of the boost converter is continuous which can reduce the size of input filter [22].
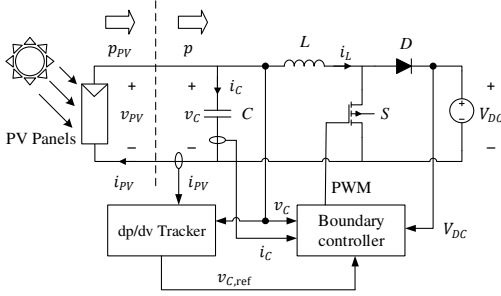
Fig. 1   The proposed control scheme with a boost-type PV converter.
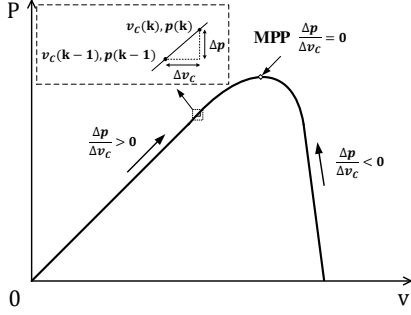
Fig. 2   PV P-V characteristic and principle of MPP tracker.

Fig. 1 shows a typical boost-type PV converter with MPPT in the proposed control scheme block diagram [23]. System input is a group of PV panels exhibiting typical PV characteristics. System output is a dc voltage source which represents a dc grid, dc link capacitors or a grid-connected voltage source inverter (VSI). If it is an AC-grid-connected system, a double line frequency ripple appears on the dc voltage source, a closed loop system is required to avoid that to affect MPPT performance. The proposed MPPT controller composes of two control loops, namely "*dp/dv* tracker" as the outer loop and "boundary controller" as the inner loop. The *dp/dv* tracker traces the MPP along the PV characteristic by calculating the instant slope of the curve. It delivers a voltage reference to the inner loop controller to keep the converter operating at or around the point. The inner loop controller employs the concept of boundary control with second-order switching surface, which exhibits very fast dynamic responses to track the operating point. Therefore, the overall controller can track the MPP in a fast and accurate way.

A. dp/dv Tracker Algorithm

In this paper, the applied *dp/dv* tracker is developed from the incremental conductance method. The slope of power and voltage curve is constantly calculated to track the maximum power point of PV panels. Sensor circuit acquires the instantaneous output voltage and current of the PV cell and therefore the power of PV array p_{PV} is given in the following equation,

$$p_{PV} = v_{PV} \times i_{PV}, \tag{1}$$

where p_{PV}, v_{PV}, and i_{PV} are output power, output voltage and output current of PV panels as defined in Fig. 1.

The boost converter in Fig. 1 interfaces the PV panel in dc form. The time-varying input capacitor voltage, $v_C(k)$ and input

power of the converter, $p(k)$, are identical to the output voltage and output power of the PV panels, v_{PV} and p_{PV} respectively. The input power of the converter, $p(k)$, is calculated by the product of $v_C(k)$ and PV output current, $i_{PV}(k)$,

$$p(k) = v_C(k) \cdot i_{PV}(k). \tag{2}$$

The slope of P-V curve can be obtained by two consecutive points on the curve,

$$\frac{\Delta p}{\Delta v_C} = \frac{p(k) - p(k-1)}{v_C(k) - v_C(k-1)}, \tag{3}$$

where $v_C(k)$ and $v_C(k-1)$ represent capacitor voltage, $p(k)$ and $p(k-1)$ are output power of PV panels of two consecutive moments.

The continuous-time signal is approximated by the interpolation of the discrete signal, i.e. $\frac{dp}{dv_C} = \frac{\Delta p}{\Delta v_C}$. The MPP tracking strategy on the P-V curve is illustrated in Fig. 2. An integrator is employed in this loop of control to eliminate the steady error of MPP.
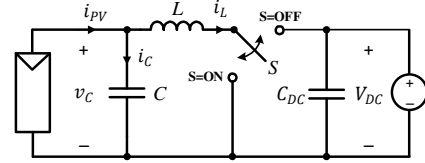
Fig. 3   Equivalent circuit of PV converter.
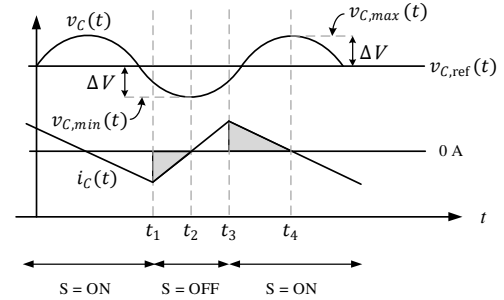
Fig. 4   Capacitor voltage and current waveforms in the steady state.

B. Control Laws of Boundary Control with Second-order Switching Surface

The boundary control family includes first-order switching surface such as sliding mode control [24] and hysteresis control, and the main advantage is inherently stable [25]-[26]. However, dynamic performance of first-order boundary controller is limited [21]. To provide a fast and precise control towards targeting output voltage in the inner loop, a boundary controller with second-order switching surface is used in this paper [27]-[30]. The boundary controller is actualized by governing voltage ripple of PV output voltage, where the ripple band of capacitor voltage are confined by two consecutive switching actions. Criteria of such switching moments are derived from the equilibrium states of the converter operations.

Schematic of PV converter with MPPT controller is depicted in Fig. 1. In the equivalent circuit, the converter is shown with two operational states which is the switch S is turned ON and OFF as shown in Fig. 3. Fig. 4 provides a graphic illustration of the ideal input capacitor voltage and current waveforms of a boost converter. Both capacitor current and voltage are captured by the converter sensors circuit. According to the second-order

boundary control law, the switch Turning-OFF moment at time instant t_1 is able to be predicted by using the capacitor current crossing zero information and the system parameter when the capacitor voltage reaching $v_{C,min}$ at the time instant t_2. It employs the geometry of capacitor voltage and current curves. Turning-OFF criteria of the switch can be derived as,

$$v_C(t) \leq v_{C,min} + \left[\frac{L}{2C}\frac{1}{v_{DC}-v_C}\right] i_C^2(t), \qquad (4)$$

and

$$i_C(t) \leq 0. \qquad (5)$$

Similarly, Turning-ON criteria of the switch is determined by the capacitor current crossing zero information and the system parameter when the capacitor voltage reaching $v_{C,max}$ at the time instant t_4. By applying the same analytical method as in Turning-OFF criteria, Turning-ON criteria is therefore expressed as,

$$v_C(t) \geq v_{C,max} - \left[\frac{L}{2C}\frac{1}{v_C}\right] i_C^2(t), \qquad (6)$$

and

$$i_C(t) \geq 0. \qquad (7)$$

The Turning-OFF and Turning-ON criteria in (4) – (7) are inequality, which can be easily implemented by the digital microcontroller [29]. The boundary control law in a discrete system is illustrated in Fig. 5.

Unlike PI controller uses past information to provide the control signal, the boundary controller is based on the criteria (4) – (7) and prediction to provide control with boundaries ($v_{C,min}$, $v_{C,max}$) of the control target. Thus, it provides fast dynamic responses.
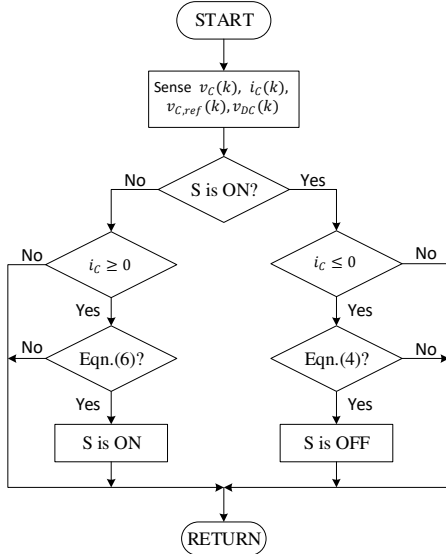
Fig. 5   Boundary control law in a discrete system.

III. STEADY STATE CHARACTERISTICS OF PV SYSTEM

This section is aimed to perform the steady state analysis of the proposed scheme. Based on a single diode model [31], the mathematical model of a PV cell is studied and is shown in Fig. 6. Comparisons of theoretical calculations with simulation results in steady state are evaluated in this section.

A. PV Array I-V Characteristics

In order to simplify the model of PV panels, equivalent series resistance R_S and equivalent parallel resistance R_P are neglected in this paper. I-V characteristic of PV array in the nominal working condition where irradiance of sun $E_n = 1000W/m^2$ and temperature $T_n = 25°C$ is constituted in following equation [32],

$$i_{PV} = N_p I_{sc,n} - I_{0,n}\left[\exp\left(\frac{v_{PV}}{N_s aV_{T,n}}\right) - 1\right], \qquad (8)$$

where N_p is number of PV panels in parallel, N_s is number of PV panels in series, $I_{sc,n}$ is nominal short-circuit current, $I_{0,n}$ is saturation current of photovoltaic and its equation is given in Appendix, a is the ideality factor of diode which is typically between 1 to 2 and it is chosen as 1 in this paper for simplifying the equation and finally $V_{T,n}$ represents thermal voltage.

By taking the approximation that the exponential component is significantly greater than 1, i.e. $\exp\left(\frac{v_{PV}}{N_s aV_{T,n}}\right) \gg 1$, (8) can be simplified as,

$$i_{PV} = N_p I_{sc,n} - I_{0,n}\exp\left(\frac{v_{PV}}{N_s aV_{T,n}}\right). \qquad (9)$$

A typical PV I-V curve is shown in Fig. 7 and it can be graphically represented by (9). Provided that the MPP of the PV cell is located at Point 1. According to (9), the slope at the MMP can be determined by the reciprocal of the instant output resistance of PV cell and is expressed as,

$$\frac{1}{r_{PV}} = \frac{di_{pv}}{dv_{pv}} = -\frac{I_{0,n}}{N_s aV_{T,n}}\exp\left(\frac{V_{PV}}{N_s aV_{T,n}}\right), \qquad (10)$$

or

$$\frac{1}{r_{PV}} = \frac{di_{pv}}{dv_{pv}} = \frac{I_{PV}-N_p I_{sc,n}}{N_s aV_{T,n}}. \qquad (11)$$

In principle, (10) and (11) apply to all the points on the I-V curve, including point 2 and 3. By substituting a steady state value of V_{PV} or I_{PV} into (10) or (11) respectively, the small signal PV output conductance can be easily obtained with physical parameters of PV panels. From (10), the relationship of the change of v_{PV} and i_{PV} is negative, thus it can be estimated that ripple polarities of voltage and current are opposite and current ripple in steady state is able to be approximated by (11).
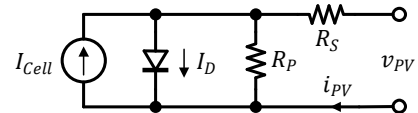
Fig. 6   The Single-diode model equivalent circuit of a PV cell [31].
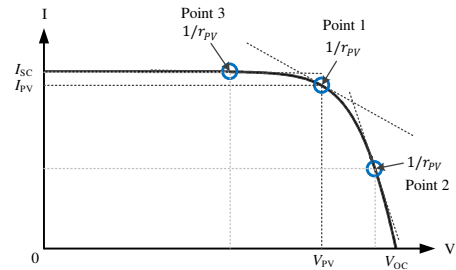
Fig. 7   A typical PV I-V curve.

B. Capacitor Voltage Ripple

In the boundary controller, ΔV is a fixed value which represented the voltage band of the filter capacitor voltage. As shown in Fig. 4, the actual peak-to-peak voltage ripple ΔV_C is the addition of ΔV_{ref} and $2\Delta V$ as,

$$\Delta V_C = \Delta V_{ref} + 2 \cdot \Delta V. \qquad (12)$$

When the integrator gain K_I of outer loop controller is properly chosen, steady error will be zero, thus $\Delta V_{ref} \cong 0$, so capacitor voltage ripple is actually band of boundary control.

C. PV Output Current Ripple

The amplitude of PV output current ripple is determined by the PV I-V characteristics. And it can be obtained from (10),

$$\Delta I_{PV} = \Delta V_c \frac{I_{0,n}}{N_s a V_{T,n}} \exp\left(\frac{V_{PV}}{N_s a V_{T,n}}\right). \quad (13)$$

D. System Operation Frequency

As shown in Fig. 4, the absolute peak value of inductor current remains identical during switch Turning-ON and Turning-OFF in steady state, thus duty ratio is calculated as,

$$D = \frac{V_{DC} - v_C}{V_{DC}}. \quad (14)$$

Inductor current ripple (peak-to-peak) is described as,

$$\Delta i_L = \frac{v_C D}{fL}. \quad (15)$$

One feature of boundary controller is varying switching frequency since there is no clock to govern the switching period. The operation frequency is

$$f = \sqrt{\frac{v_C D}{8LC\Delta V_C}}. \quad (16)$$

Based on (16), the system operation frequency can be found. By varying the capacitor band, different operation frequency can be generated.

IV. SIMULATION RESULTS

A. Steady State Operation

This section compares the calculation results of PV model with simulation results. The topology with dual control loops shown in Fig. 1 is implemented in simulation with PLECS software. Both theoretical calculation and software simulation use the same parameters of the circuits as shown in Table I.

A 2×2 PV array is used in simulation as the input power source, capacitor voltage, PV output current, inductor current and gate signal at steady state are illustrated in Fig. 8. Using given parameters listed in Table I, theoretical values in the steady state are calculated by equations given in the previous section. Table II compares calculated values in the steady state with simulation results in steady state. This table indicates that the simulation results match theoretical calculations.

B. Transient Performance

A comparative study of the transient performance of proposed controller and a conventional PI-based MPPT controller is performed in simulation. Parameters of both controllers are shown in Table III. A step change of irradiance of the sun is applied to both controllers simultaneously. Dynamic response of proposed controller and conventional PI controller in the simulation are depicted in Fig. 9, where the green colour waveforms are generated by the proposed controller and the red colour ones are created by the conventional PI controller. Both controllers share the same outer loop, the *dp/dv* tracker. Both controllers can successfully track the MPP after the irradiation step changes. However, the PI controller needs much more switching cycles to reach the new MPP, since the converter passive component responses are

included in the transfer functions in the control loop. This slow response characteristic leads to reducing MPPT efficiency during the transient. Contradictorily, the proposed controller can respond at once to govern the converter to achieve maximum power extraction. The results show that the dynamic response of MPPT is depended on the inner control loop. It generates approximate 30mJ more in each transient in the simulation.
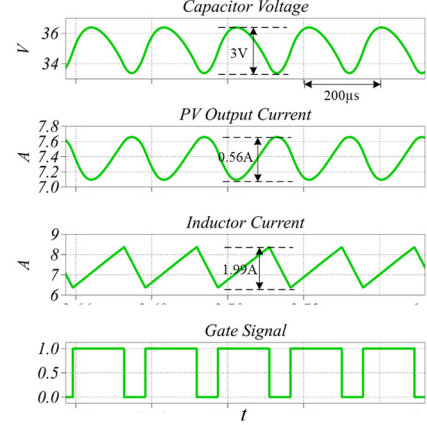
Fig. 8   Simulation waveforms in steady state.

Table I
Parameters for Theoretical Calculation

Parameters	Values	Parameters	Values
N_p	2	N_s	2
$I_{sc,n}$	3.99 A	$V_{oc,n}$	22.05 V
V_T	1.852 V	a	1
L	2.4 mH	C	15 μF
ΔV	1.5 V		

Table II
Simulation and Theoretical Values in Steady State

Parameter	Simulation Results	Theoretical Values
V_{MPP}	34.88 V	35.374 V
I_{MPP}	7.38 A	7.22 A
ΔV_C	3 V	3 V
ΔI_{PV}	0.56 A	0.61 A
duty ratio	0.708	0.705
ΔI_L	1.99 A	1.93 A
f	5263 Hz	5373 Hz

Table III
Proposed MPPT vs PI Based MPPT Simulation Results

System Parameter	Proposed MPPT	Conventional PI Based MPPT
Inductance	2.4 mH	
Capacitance	15 μF	
Output voltage	120 V	
Sun irradiance change	From 50% to 100%	
Simulation time	0.04 S	
Voltage ripple(p-p)	3 V	
Switching frequency	4974-5165 Hz	5000 Hz
PI parameters	N/A	K_P:0.008, K_I:20
Settling time	300 us	3 ms

Fig. 10 is the corresponding X-Y plot of capacitor voltage and inductor current in the simulation. The PV characteristic is changed from Line 2 to Line 1. The system operates in the steady state before and after the transient and at the MPP of the I-V curves. During the transient, the system follows the Turn-on

trajectory (red solid line) toward the new operating point. While the system reaches the Turn-off trajectory (blue dash line) which can operate at the new MPP, the system operates in steady state (oscillating around the MPP with the Trajectories) and governed by the boundary controller. Therefore, the system can achieve the steady state in two switching actions.
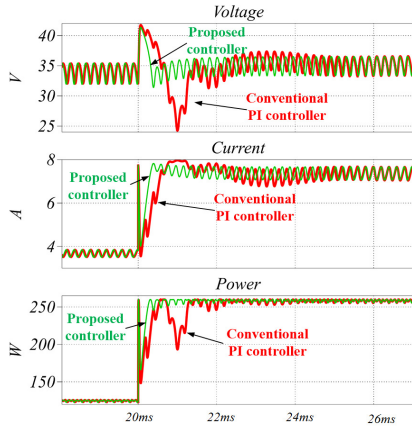
Fig. 9   Dynamic response of PI and boundary controllers based MPPT.
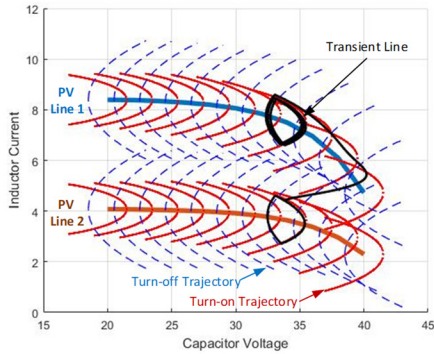
Fig. 10   MPPT moving trajectories.

Table IV
Specification of The PV Converter Prototype

Circuits parameters	Nominal values
Input capacitance C_1	15 μF
Output capacitance C_2	470 μF
Inductance L	2.4 mH
Resistance R	33.3 Ω
dc source voltage	120 V
PV panel parameters	Values
Number of series cells	36
Maximum power rating P_{MAX}	75W
Rated current I_{MPP}	4.4 A
Rated voltage V_{MPP}	17.0 V
Short circuit current I_{SC}	4.8 A
Open circuit voltage V_{OC}	21.7 V
Controller parameters	Values
CPU Clock frequency	200 MHz
ADC sampling frequency	3.5 MHz
Switching frequency	3.7-5 kHz

V.   EXPERIMENTAL VERIFICATIONS

A. Experimental Setup

A 280W boost-type PV converter prototype has been implemented. It was embedded with a DSP based MPPT controller to experimentally verify the proposed concept. As shown in Fig. 11 (a), the input of the converter consists of a group of 2 × 2 PV panels which are connected to the converter via a long cable. Resistors and the dc voltage source are parallel connected to the output. The overview of the testbed is shown in Fig. 11 (b). A dc voltage source is connected to the output and is used to control the dc link voltage. Resistors are applied to the output as loading of the system. Under different environment situations, the converter can adjust to the maximum PV power point in a short period of time. Circuit parameters, PV panel parameters and controller parameters are listed in Table IV.

(a)

(b)
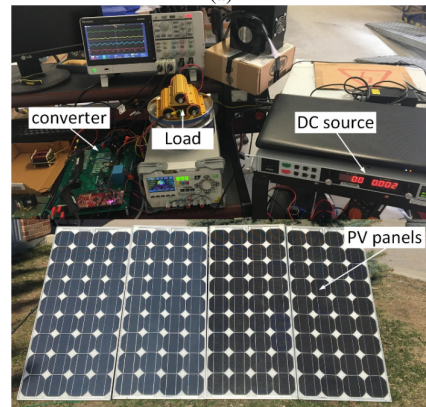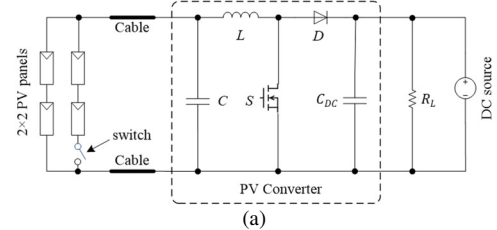
Fig. 11   Testbed (a) schematic of testbed, and (b) laboratory setup.

(a)

(b)
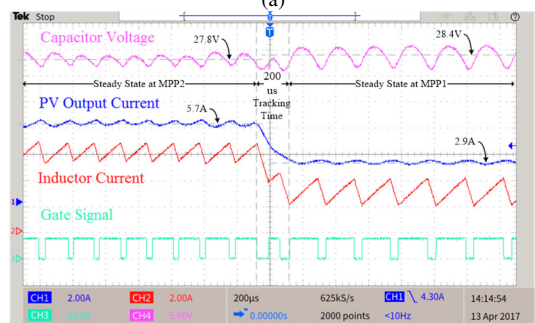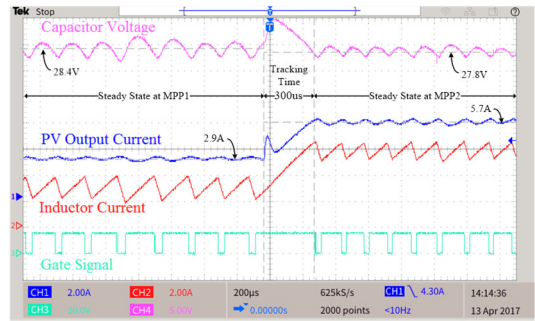
Fig. 12   Experiment results of a step change of (a) switched from 2 to 4 panels, and (b) vice versa.
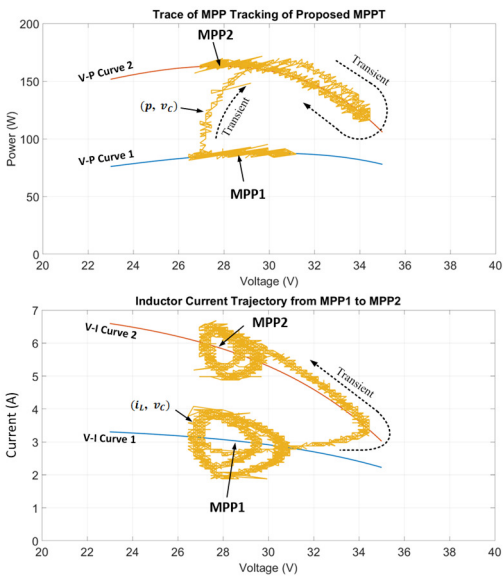
Fig. 13   Power and Inductor current trajectories for Fig. 12 (a).

B. Experimental Results – Transient Performance

Fig. 12 shows the dynamic response of the PV system from two PV panels in series to two PV strings in parallel where each of them includes two PV panels in series. The transient response of the MPPT controller is evaluated by switching on and off of one PV string branch. Once the other PV string is in operation, new MPP is supposed to be reached immediately. Fig. 12 (a) and (b) explicate the behavior of the system output under a step change in the number of connecting PV modules suddenly. From Fig. 12 (a), PV output current suddenly rises to its double quantity when the second PV string is switched on. From capacitor voltage waveform, it can be found that new MPP is getting stabilized in one switching cycle around 300us. Similarly, in Fig. 12 (b), the connection is switched from 2×2 to 1×2 PV array where the capacitor voltage is stabilized in two switching actions with 200us. The input current is dramatic dropped to an approximately 50% of its previous value. The corresponding switching trajectory of Fig. 12 (a) is shown in Fig. 13 where the inductor current is in yellow color. The controller manages to catch the new operating point in one switching action on the estimated I-V curve. Also, the new MPP is reached with estimated P-V curve in one switching action.

VI. Conclusion

In this paper, a fast MPPT control scheme for PV application was presented. In the proposed method, a *dp/dv* tracker algorithm is coordinated with a boundary controller to achieve a fast dynamic tracking performance. The proposed control scheme has a significant improvement compared to the conventional PI-based MPPT method. The control scheme allows a boost-type PV converter to extract more energy from PV cells during irradiation change. The design of the proposed MPPT controller is supported with theoretical interpretation. The boundary control laws of a boost converter with input voltage control and the entire system steady state characteristics have been determined. A laboratory prototype is built based on a boost-type converter with a DSP controller. Experiment results show that the proposed controller responds quickly (300us)

during transients to locate at the new MPP. The results matched with the conceptual idea and the derived theory.

References

[1] Y. Zhou, C.N.M. Ho, K.K.M. Siu, "A fast and accurate MPPT control technique using boundary controller for PV applications." *Proc. IEEE APEC*, pp. 2822-2829, 2017.

[2] G. K. Singh, 'Solar power generation by PV (photovoltaic) technology: A review', *Energy*, vol. 53, pp. 1–13, May 2013.

[3] J. L. Smith, "Photovoltaics", *Science*, vol. 212, no. 4502, pp. 1472-1478, 1981.

[4] J. Ayoub, "National Survey Report of PV Power Applications in Canada", *International Energy Agency*, 2006.

[5] C. Ho, "Challenges and design considerations of PV inverters in the future Smart Grids," *IET APSCOM12*, Nov. 2012.

[6] Y. Zhou, C. Ho, "A review on Microgrid architectures and control methods," *Proc. IEEE ECCE-Asia*, pp. 3149 – 3156, 2016.

[7] H. Patel and V. Agarwal, "Maximum power point tracking scheme for PV systems operating under partially shaded conditions," *IEEE Trans. Ind. Electron*, vol. 55, no. 4, pp. 1689–1698, Apr. 2008.

[8] M. Metry, M.B. Shadmand, R. S. Balog and H. A. Rub, "MPPT of Photovoltaic Systems Using Sensorless Current-Based Model Predictive Control" *IEEE Trans. Ind. Electron*, vol. 53, no. 2, pp. 1157-1167, 2016.

[9] EN 50530: *Overall efficiency of grid connected photovoltaic inverters*, April 2010.

[10] E. Mamarelis, G. Petrone, G. Spagnuolo, "A two-steps algorithm improving the P&O steady state MPPT efficiency," *Applied Energy*, vol. 113, pp. 414–21, Jan 2014.

[11] N. Femia, G. Petrone, G. Spagnuolo, and M. Vitelli, "Optimization of perturb and observe maximum power point tracking method," *IEEE Trans. Power Electron*., vol. 20, no. 4, pp. 963–973, 2005.

[12] H. A. Sher, A. A. Rizvi, K. E. Addoweesh and K. Al-Haddad, "A Single-Stage Stand-Alone Photovoltaic Energy System With High Tracking Efficiency," *IEEE Trans. Sustain. Energy.,* vol. 8, no. 2, pp. 755–762, 2017.

[13] J. Ahmed and Z. Salam, "A Modified P&O Maximum Power Point Tracking Method With Reduced Steady-State Oscillation and Improved Tracking Efficiency," *IEEE Trans. Sustain. Energy.,* vol. 7, no. 4, pp. 1506 - 1515, 2016.

[14] I. S. Kim, M. B. Kim, and M. J. Youn, "New maximum power point tracker using sliding-mode observer for estimation of solar array current in the grid-connected photovoltaic system," *IEEE Trans. Ind. Electron*., vol. 53, no. 4, pp. 1027–1035, 2006

[15] N. E. Zakzouk; M. A. Elsaharty; A. K. Abdelsalam; A. A. Helal and B. W. Williams; "Improved performance low-cost incremental conductance PV MPPT technique," *IET Renew. Power Gener.*, vol. 10; no. 4, pp. 561-574, 2016.

[16] M. A. G. de Brito, L. Galotto, L. P. Sampaio, G. de Azevedo e Melo, and C. A. Canesin, "Evaluation of the main MPPT techniques for photovoltaic applications," *IEEE Trans. Ind. Electron*., vol. 60, no. 3, pp. 1156–1167, Mar. 2013.

[17] B. Alajmi, K. Ahmed, S. Finney, and B. Williams, "Fuzzy logic controlled approach of a modified hill climbing method for maximum power point in microgrid stand-alone photovoltaic system," *IEEE Trans. Power Electron*., vol. 26, no. 4, pp. 1022–1030, Apr. 2011.

[18] M. A. Elgendy, B. Zahawi, and D. J. Atkinson, "Assessment of perturb and observe MPPT algorithm implementation techniques for PV pumping applications," *IEEE Trans. Sustain. Energy*, vol. 3, no. 1, pp.21–33, Jan. 2012.

[19] M. Pokharel, A. Ghosh, and C. Ho, "Small-Signal Modelling and Design Validation of PV-Controllers with INC-MPPT using CHIL", *IEEE Trans. on Energy Conversion*, (Early Access).

[20] G. Velasco-Quesada, F. Guinjoan-Gispert, R. Pique-Lopez, M. Roman-Lumbreras and A. Consea-Roca, "Electrical PV Array Reconfiguration Strategy for Energy Extraction Improvement in Grid-Connected PV Systems," *IEEE Trans. Ind. Electron*, vol. 56, no. 11, pp. 4319-4331, Nov. 2009.

[21] C. Ho, H. Breuninger, S. Pettersson, G. Escobar and F. Canales, "A comparative performance study of an interleaved boost converter using commercial Si and SiC diodes for PV applications", *IEEE Trans. Power Electron*, Vol. 28, No. 1, pp. 289 – 299, Jan. 2013.

[22] W. Xiao, N. Ozog, and W. G. Dunford, "Topology study of photovoltaic interface for maximum power point tracking," *IEEE Trans. Ind. Electron*, vol. 54, no. 3, pp. 1696–1704, Jun. 2007.

[23] C. Ho, H. Breuninger, S. Pettersson, G. Escobar, L. Serpa, and A. Coccia, "Practical design and implementation procedure of an interleaved boost converter using SiC diodes for PV applications", *IEEE Trans. Power Electron*, Vol. 27, No. 6, pp. 2835 – 2845, Jun. 2012.

[24] Messikh, T., Rahim, N., Saad, M.: 'Boundary control of dual-output boost converter using state-energy', *IET Power Electron.*, Vol. 7, pp. 2310–2321, Sep. 2014.

[25] N. Keskar and G. A. Rincon-Mora, "Self-stabilizing, integrated, hysteretic boost DC-DC converter," *Proc. IEEE IECON*, pp. 586-591 Vol. 1, 2004.

[26] S. Dietrich, R. Wunderlich and S. Heinen, "Stability Considerations of Hysteretic Controlled DC-DC Converters," *Proc. PRIME,* pp. 1-4, 2012.

[27] W. W. Burns, III and T. G. Wilson, "System-state and operating condition sensitive control method and apparatus for electric power delivery systems," *U.S. Patent 4084103 A*, Apr 11, 1978

[28] K. K. S. Leung and H. Chung, "State trajectory prediction control for boost converters" *Proc. IEEE ISCAS '04, vol. 5, pp. 556-559, May 2004.*

[29] K. Au, C. Ho, H. Chung, W.H. Lau and W.T. Yan "Digital implementation of boundary control with second-order switching surface for inverters", *Proc. IEEE PESC07, Jun. 2007.*

[30] C. Ho, H. Chung, and K. Au, "Design and implementation of a fast dynamic control scheme for capacitor-supported dynamic voltage restorers," *IEEE Trans. Power Electron.*, vol. 23, no. 1, pp. 237-251, Jan. 2008.

[31] M. G. Villalva, J. R. Gazoli, and E. R. Filho, "Comprehensive approach to modeling and simulation of photovoltaic arrays," *IEEE Trans. Power Electron.*, vol. 24, no. 5, pp. 1198–1208, May 2009.

[32] H. Cai, J. Xiang and W. Wei, "Modelling, analysis and control design of a two-stage photovoltaic generation system," *IET Renew. Power Gener.*, vol. 10, no. 8, pp. 1195-1203, 9 2016.

VII. APPENDIX

A. Derivation of (4) and (6)

In Fig. 3 (a), the switch S is in ON state and the diode D is in OFF state. Thus, inductor L is charging up from the PV source and part of PV output current goes to C_1 according to KCL [27]. As a result, the following equations can be derived.

$$i_L = i_{PV} - i_C \qquad (A1)$$

And
$$v_L = v_C \qquad (A2)$$

where i_L, i_{PV} and i_C are inductor current, PV output current and capacitor current respectively. And v_L is the voltage over inductor and v_C is the voltage of capacity C. Since i_{PV} is assumed as a dc current, derivative of (A1) can result in the following equations,

$$\frac{di_L(t)}{dt} \cong -\frac{di_C(t)}{dt} \qquad (A3)$$

$$v_L(t) = L\frac{di_L(t)}{dt} \qquad (A4)$$

By combining (A2) – (A4), capacitor voltage can be rearranged as follows.

$$v_C = \frac{1}{C}\int i_C(t)dt + v_C(0) \qquad (A5)$$

where $v_C(0)$ represents capacitor initial voltage. (A4) can be rearranged as

$$dt = \left|L\frac{di_C}{v_C}\right| \qquad (A6)$$

As capacitor voltage equals to the initial voltage, the instantaneous voltage at t_3, plus with the integration of capacitor current from t_3 to t_4 which is the triangular shadow area in capacitor current waveform within the time interval of t_3 and t_4 in Fig. 6. Therefore, integral of capacitor current can be simplified as,

$$\int_{t_3}^{t_4} i_C(t)dt = \frac{1}{2}i_C(t_3)\Delta t \qquad (A7)$$

The crest value of capacitor voltage waveform can be obtained by putting (A6) and (A7) into (A5), as such

$$v_{C,max} = v_C(t_4) = \left[\frac{L}{2C}\frac{1}{v_C}\right]i_C^2(t_3) + v_C(0) \qquad (A8)$$

where $v_{C,max}$ is upper peak reference capacitor voltage. Therefore, turn-on criteria of S must fulfill (A8), thus an inequality (6) can be derived.

Similarly, in Fig. 3 (b), the switch S is in OFF state and the diode D is in ON state. Thus, inductor L is discharging and delivering to the output capacitor C_{DC} and the output dc source. Thus, the voltage across the inductor is the difference of input voltage, v_C, and output voltage, v_{dc}, The value of capacitor voltage $v_{C,min}$ can be derived as,

$$v_{C,min} = v_C(t_2) = -\left[\frac{L}{2C}\frac{1}{v_{dc}-v_C}\right]i_C^2(t_1) + v_C(0) \qquad (A9)$$

where $v_{C,min}$ is lower peak reference capacitor voltage. Therefore, turn-off criteria of S must fulfill (A9), thus an inequality (4) can be derived.

B. Derivation of (10) and (11)

By using (9), and introducing small signals,

$$I_{PV} + i_{pv} = N_p I_{sc,n} - I_{0,n}\exp\left(\frac{V_{PV}+v_{pv}}{N_s aV_{T,n}}\right) \qquad (A10)$$

By taking the derivative,

$$\frac{di_{pv}}{dv_{pv}} = -\frac{I_{0,n}}{N_s aV_{T,n}}\exp\left(\frac{V_{PV}}{N_s aV_{T,n}}\right)\exp\left(\frac{v_{pv}}{N_s aV_{T,n}}\right) \qquad (A11)$$

Assume the small signal of v_{pv} is much smaller than the steady state voltage V_{PV}, i.e. $v_{pv} \ll V_{PV}$, (10) can be obtained. By putting (9) into (10), then (11) can be obtained, where

$$I_{0,n} = \frac{N_p I_{sc,n}}{\exp\left(\frac{V_{oc,n}}{aV_{T,n}}\right)-1} \qquad (A12)$$

C. Derivation of (13)

By using (12), and introducing small signals,

$$P_{PV} + p_{pv} = (V_{PV} + v_{pv})N_p I_{sc,n} - \\ (V_{PV} + v_{pv})I_{0,n}\exp\left(\frac{V_{PV}+v_{pv}}{N_s aV_{T,n}}\right) \qquad (A13)$$

By taking the derivative,

$$\frac{dp_{pv}}{dv_{pv}} = N_p I_{sc,n} - I_{0,n}\left(1 + \frac{V_{PV}+v_{pv}}{N_s aV_{T,n}}\right)\exp\left(\frac{V_{PV}+v_{pv}}{N_s aV_{T,n}}\right) \qquad (A14)$$

Assume the small signal of v_{pv} is much smaller than V_{PV}, i.e. $v_{pv} \ll V_{PV}$, thus, (13) can be obtained.